Suppression of aliasing in multi-sensor scanning absolute profile measurement

Axel Wiegmann,[1,2,*] Michael Schulz[1] and Clemens Elster[2]

[1]*Physikalisch-Technische Bundesanstalt, Bundesallee 100, 38116 Braunschweig, Germany*
[2]*Physikalisch-Technische Bundesanstalt, Abbestr. 2-12, 10587 Berlin, Germany*
[*]*axel.wiegmann@ptb.de*

Abstract: The task of anti-aliasing in absolute profile measurement by multi-sensor scanning techniques is considered. Simulation results are presented which demonstrate that aliasing can be highly reduced by a suitable choice of the scanning steps. The simulation results were confirmed by results obtained for interferometric measurements (Nyquist frequency 1/646 μm^{-1}) on a specifically designed chirp specimen with sinusoidal waves of amplitude 100 nm and wavelengths from 2.5 mm down to 19 µm.

OCIS codes: (120.0120) Instrumentation, measurement, and metrology; (120.3180) Interferometry; (120.3940) Metrology; (120.6650) Surface measurements, figure; (100.3008) Image recognition, algorithms and filters.

References and links

1. L. Deck and P. de Groot, "High-speed noncontact profiler based on scanning white-light interferometry," Appl. Opt. **33**, 7334-7338 (1994).
2. L. Lahousse, S. Leleu, J. David, O. Gibaru, S. Ducourtieux, "Z calibration of the LNE ultra precision coordinate measuring machine," in *Proceedings of the 9th international conference of the european society for precision engineering and nanotechnology*, V 2, 348-353 (2007).
3. J. Cohen-Sabban and D. Reolon, "Vibration insensitive 3D-profilometry: a new type of white light interferometric microscopy" Proc. SPIE **7064**, (2008).
4. D J Whitehouse, "Some theoretical aspects of error separation techniques in surface metrology," J. Phys. E Sci. Instrum. **9,** 531-536 (1976).
5. W. Gao and S. Kiyono, "High accuracy profile measurement of a machined surface by the combined method," Measurement **19**, 55-64 (1996).
6. C. Elster, I. Weingaertner, and M. Schulz, "Coupled distance sensor systems for high-accuracy topography measurement: Accounting for scanning stage and systematic sensor errors," Prec. Eng. **30**, 32–38 (2006).
7. A. Wiegmann, M. Schulz, and C. Elster, "Absolute profile measurement of large moderately flat optical surfaces with high dynamic range, " Opt. Express **16**, 11975-11986 (2008), http://www.opticsinfobase.org/oe/abstract.cfm?URI=oe-16-16-11975.
8. µPhase Interferometer, FISBA Optik AG, CH-9016 St. Gallen and FISBA Optik GmbH, Berlin, http://www.fisba.ch/.
9. MPLS 180, STIL - 595, rue Pierre Berthier - Domaine de Saint Hilaire - 13855 Aix en Provence Cedex 3 – FRANCE, http://www.stilsa.com/.
10. E. Marsh, J. Couey, and R. Vallance, "Nanometer-Level Comparison of Three Spindle Error Motion Separation Techniques," J. Manuf. Sci. Eng. **128**, 180-187 (2006)
11. V. Bakshi, *EUV Lithography* (John Wiley & Sons, 2009), Chap. 5.3
12. B. Doerband and J. Hetzler, "Characterizing lateral resolution of interferometers: the Height Transfer Function (HTF)," Proc. SPIE **5878**, 587806 (2005).
13. R. Krueger-Sehm, P. Bakucz, L. Jung, H. Wilhelms, "Chirp-Kalibriernormale fuer Obeflaechenmessgeraete". Technisches Messen **74,** 572-576 (2007).
14. A. Wiegmann, C. Elster, M. Schulz, M. Stavridis, "Absolute Topographievermessung gekruemmter optischer Oberflaechen mit hoher lateraler Aufloesung", in *Proceedings of the 109th DgaO,* http://www.dgao-proceedings.de/download/109/109_p28.pdf.

#109895 - $15.00 USD Received 8 Apr 2009; revised 7 Jun 2009; accepted 11 Jun 2009; published 18 Jun 2009

1. Introduction

Topography measurement is an essential part in the production process of optical surfaces used to control the polishing process. For many surfaces such as, e.g., synchrotron optics, profile measurements are sufficient. To this end, various distance sensors are available showing sensitivities in the nanometer range [1-3]. However, when profile measurements with an uncertainty in the nm range are required, height deviations of the scanning stage have to be accounted for. Arrays of distance sensors provide redundant information which can be used to compensate the errors of the scanning stage [4,5]. A recently published profile measurement method [6,7] using a distance sensor array is capable to measure absolute profiles with an uncertainty in the region of the sensitivity of the distance sensors, while height and tilt errors of the scanning stage as well as systematic errors of the sensor array are accounted for. This technique can be employed with commercially available types of distance sensor arrays [8,9]. Alternatively, also single sensors can be used to design a suitable sensor array [2].

Ideally, the topography heights are reconstructed exactly at discrete measurement positions which are usually chosen equidistantly. However, in this case the topography between the measurement positions can be exactly interpolated only when the topography contains no wavelengths shorter than twice the distance between adjacent measurement positions. Otherwise, aliasing will emerge, i.e. the interpolated topography will differ from the real one. Imaging quality of high precision optical surfaces is influenced by all spatial frequencies. Precise and unbiased knowledge about all of these frequencies is important to characterize the optical surface and for subsequent corrections of the specimen (ion beam edging, polishing ...). Such post processing requires interpolation of discrete topography measurements. For aliased measurement data this can cause extensive form errors and it is therefore advantageous for these and other [10] applications to avoid aliasing effects, i.e. to not exactly reconstruct the topography at the discrete set of measurement positions but to reconstruct only that part of the topography containing wavelengths longer than twice the measurement positions. Imaging systems as used in interferometers for topography measurements provide the opportunity to carry out an analogous Fourier transformation. Hence, aliasing can be suppressed in such measurement devices with a suitable chosen aperture in the Fourier plane of the imaging system [11]. Such procedure is not feasible for all types of sensors used for inspection of high precision optics resulting in aliased measurement data [12]. For a sensor array consisting of nearly punctual sensors internal suppression of aliasing is also not possible. Nevertheless, in the following, a method for reduction of aliasing for an absolute profile measurement by a multi-sensor scanning procedure is proposed. The idea is to choose the measurement positions in such a way that aliasing effects are highly reduced or even eliminated. This is demonstrated by the results obtained for simulations (Section 4) as well as for measurements (Section 5). The proposed technique is applicable to all line sensors arrays with equidistant distance sensors.

2. Absolute profile measurement by a multi-sensor scanning technique

Figure 1 shows the recently proposed measurement principle [7] for traceable absolute profile measurement. The sensor head consists of multiple distance sensors. This sensor head is moved over the specimen while its position is measured with an additional displacement interferometer. An autocollimator is employed to conduct tilt measurements of the sensor system at each measurement position.

#109895 - $15.00 USD Received 8 Apr 2009; revised 7 Jun 2009; accepted 11 Jun 2009; published 18 Jun 2009

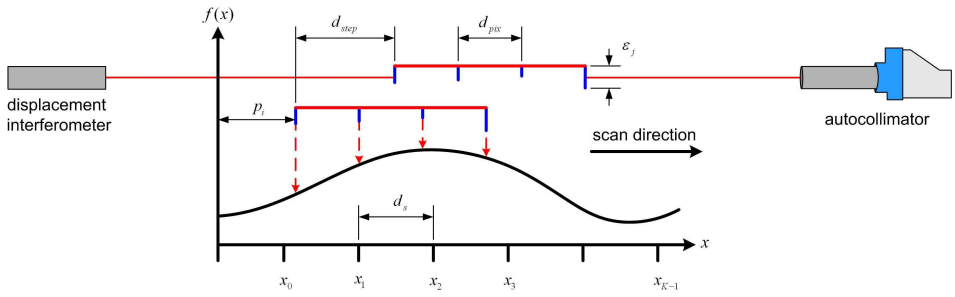

Fig. 1. Sketch of the used absolute profile measurement method. The thick red horizontal lines represent the line sensor array in different measurement positions. The blue vertical lines represent the systematic sensor errors ε_j.

In each measurement position (index i) the scanning stage leads to tilt (b_i) and offset (a_i) errors. Furthermore, each of the distance sensors shows a systematic offset error ε_j. The topography can be reconstructed at the positions x_k (k=0,1,…,K-1). It has been shown in [7] that measurement positions $\tilde{x}$ in-between the reconstruction positions can be accounted in the analysis. Applying a polynomial interpolation scheme, the data can be modeled as

$$m_{i,j} = -\sum_{k=\mathrm{floor}\left(\frac{\tilde{x}}{d_s}\right)-\frac{o-1}{2}}^{\mathrm{ceil}\left(\frac{\tilde{x}}{d_s}\right)+\frac{o-1}{2}} c_k(\tilde{x}) f(x_k) + \varepsilon_j + a_i + b_i s(j) \qquad (1)$$

where

$$c_k(\tilde{x}) = \prod_{\substack{i=\mathrm{floor}\left(\frac{\tilde{x}}{d_s}\right)-\frac{o-1}{2} \\ i\neq k}}^{\mathrm{ceil}\left(\frac{\tilde{x}}{d_s}\right)+\frac{o-1}{2}} \frac{\tilde{x}-x_i}{x_k-x_i} \quad . \qquad (2)$$

Equation (1) is linear with respect to the unknowns a_i (offsets), b_i (tilts), ε_j (systematic sensor errors) and $f(x_0),\ldots,f(x_{K-1})$ (topography). The additional tilt measurements are essential to ensure absolute profile reconstruction since otherwise the quadratic part of the topography is lost due to the unknown systematic sensor errors, cf. [6]. The reconstruction distance $d_s = x_k - x_{k-1}$ has to be larger than half of the pixel distance d_{pix}. The coefficients c_k in equation (1) are based on a polynomial interpolation with a high degree o of the interpolation polynomial. The transfer function associated with this interpolation scheme is shown in Fig. 2.

#109895 - $15.00 USD Received 8 Apr 2009; revised 7 Jun 2009; accepted 11 Jun 2009; published 18 Jun 2009

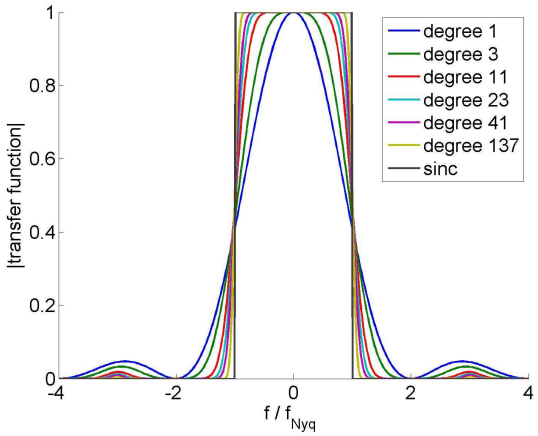

Fig. 2. Transfer functions of the interpolation scheme used in the reconstruction algorithm for different degrees of interpolation in comparison to the ideal sinc interpolation.

The higher the degree o of the interpolation polynomial the better the reconstruction of the short topography wavelengths. The interpolation interval should be chosen symmetrical to $\tilde{x}$ to obtain good results, for details cf. [7].

3. Aliasing – anti-aliasing

The measurement principle introduced in Section 2 reconstructs the topography at the discrete points x_k which form an equidistant grid with spacing d_s. In order to subsequently allow for an exact interpolation between these grid points, the topography must not contain spatial frequencies beyond the Nyquist frequency $f_{Nyq} = 1 / 2d_s$. The reason is that these higher frequencies would cause aliasing errors, i.e. they would emerge in such an interpolation as lower frequencies which are not present in the actual topography.

The profile measurements may be taken at the values x_k where the topography is reconstructed, by using $d_{step} = d_{pix}$. However, then the measurement positions are gathered at the reconstruction positions x_k and no information on the topography between the positions x_k is available. Consequently, for such proceeding aliasing cannot be controlled or reduced.

The transfer function of the reconstruction algorithm in Fig. 2 is rectangularly shaped. Therefore all frequencies smaller than f_{Nyq} are correctly reconstructed while higher frequencies are suppressed. Such behavior is ideal with respect to avoiding aliasing errors. However, Fig. 2 was calculated for continuously spaced measurement positions corresponding to an infinitesimal small scanning step d_{step}. As an approximation to this, the measurement positions of the line sensor array should be distributed as uniformly as possible. This dense sampling of the topography is then expected to approximate the ideal behavior indicated in Fig. 2 and hence to suppress the aliasing effects which are obtained for sparse sampling. Dense sampling can be realized easily as follows. For a sensor head with N equidistant distance sensors, the scanning step is chosen to $d_{step} = d_{pix} \cdot N/(N + 1)$. This results in measurement positions which are uniformly distributed in-between the reconstruction positions x_k, except for the boundaries (cf. Fig. 3).

#109895 - $15.00 USD Received 8 Apr 2009; revised 7 Jun 2009; accepted 11 Jun 2009; published 18 Jun 2009

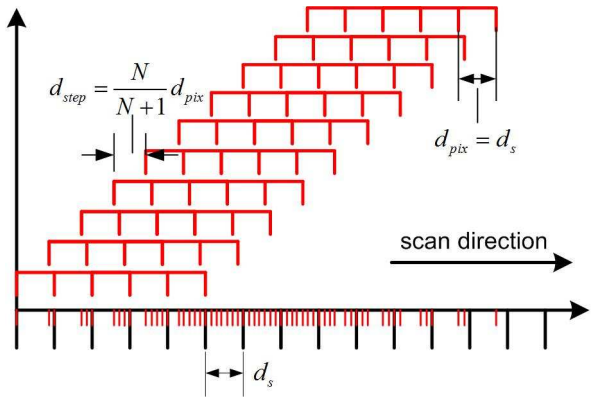

Fig. 3. Dense topography sampling with a line sensor consisting of N equidistant sensors.

Note that all single distance sensor measurements are taken at different positions and that the number of scanning steps is increased only by a factor of (N+1)/N compared to sparse sampling.

4. Simulation results

In order to assess the amount of aliasing and anti-aliasing for sparse and dense sampling, we simulated an array of N=10 distance sensors (d_{pix} = 189 µm). Measurement noise of the distance sensors (5 nm), autocollimator (0.2 arcsec (1 µrad)), distance interferometer (250 nm), positioning errors (5 µm) and tilt errors (2 arcsec (10 µrad)) of the scanning stage have been accounted for; the figures in brackets indicate the standard deviations of the (normally distributed) random variables used to simulate the various error sources. Further on, the single distance sensors have been simulated with an effective sensitive area of d_{width} = 17.96 µm leading to an averaging of the topography over a corresponding width. For the reconstruction procedure, the reconstruction distance was set to $d_s = d_{pix}$ and the degree of the interpolation polynomial to o = 41. The reconstruction algorithm described in the previous Section allows for a reconstruction only up to an arbitrary straight line. On this account, the reconstructed topography has been rotated and shifted relative to the desired topography such that the root mean square error is minimal. As test functions sinusoidal topographies with varying wavelengths and amplitude of 100 nm have been used. Since we are interested in studying aliasing effects, topography reconstruction errors were assessed as follows: For topographies consisting of frequencies smaller than the Nyquist frequency ($f_{Nyq} = 1 / 2d_s$), the usual root mean square error was used. For topographies consisting of higher frequencies the root mean square error to a flat topography was calculated, as perfect anti-aliasing would yield a flat reconstructed topography in these cases. Figure 4 shows the obtained results for sparse ($d_{step} = d_{pix}$) and for dense ($d_{step} = d_{pix} \cdot N/(N + 1)$) sampling.

#109895 - $15.00 USD Received 8 Apr 2009; revised 7 Jun 2009; accepted 11 Jun 2009; published 18 Jun 2009

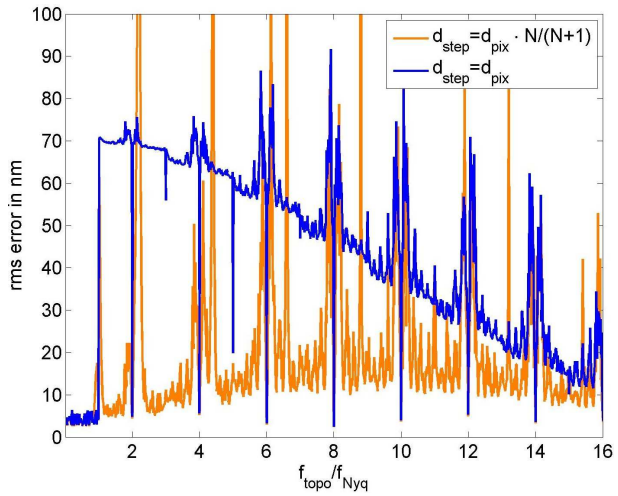

Fig. 4. Root mean square errors of the reconstructed topographies in dependence on the frequency of the simulated topography (f_{topo}) for dense and fore sparse sampling.

Sparse sampling shows strong aliasing effects for topography frequencies beyond the Nyquist frequency f_{Nyq} leading to an abrupt worsening of the reconstruction results. For higher topography frequencies, the results become better due to the low pass filtering caused by the averaging over the sensitive areas of the distance sensors. Note that topographies with $f_{topo} / f_{Nyq} = 2M$ (M=1,2,3,…) produce larger reconstruction errors than expected by simple aliasing ($\text{amplitude} \cdot 2^{-1/2}$). The reconstruction algorithm causes these errors, as it is impossible for these frequencies to decide if the measured values are due to the sinusoidal topography or a sinusoidal height error of the scanning stage. The dense sampling significantly reduces aliasing effects. The gain is nearly one order of magnitude for frequencies directly above the Nyquist frequency f_{Nyq}. But note that the aliasing errors still remain for the frequencies near to $f_{topo} / f_{Nyq} = 2M$ (M=1,2,3,…), due to the mentioned interference of these frequencies with the reconstruction algorithm, and that also some other single frequencies share aliasing errors.

5. Measurement results

In order to support the simulation results, interferometric measurements on a chirp specimen have been carried out. Since measurement results are presented in spatial domain in this Section, waviness of the specimen will be denoted in terms of wavelength instead of frequencies. Instead of a set of sinusoidal topographies covering a wide range of wavelengths, a single chirp specimen has been produced. Chirp specimens are used to characterize the lateral resolution of measurement setups [12,13] and can therefore also be used for the analysis of aliasing effects. The advanced fabrication technology-working group at PTB has manufactured the Chirp specimen. The rotational symmetric topography was fabricated in a diamond turning process on a nickel layer on a copper specimen. Starting 16 mm from the center, several single sinusoidal wavelengths have been stringed together. The largest wavelength was $\lambda = 2.5$ mm, then every following wavelength was reduced by 2% relative to the one before down to $\lambda = 1$ mm. After this point the wavelengths were reduced by a factor of $2 \cdot 10^{-4}$ down to $\lambda = 19$ µm to obtain higher resolution. Figure 5 shows the wavelengths of the chirp specimen as function of the distance to the center.

#109895 - $15.00 USD Received 8 Apr 2009; revised 7 Jun 2009; accepted 11 Jun 2009; published 18 Jun 2009

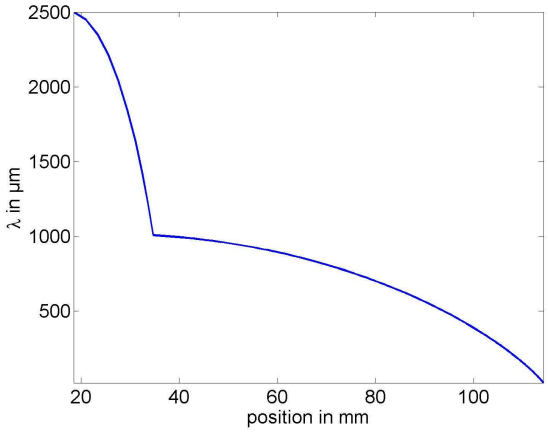

Fig. 5. Local wavelength λ of the manufactured chirp specimen as function of the distance to the center of the specimen.

The sensor head used for the measurements was a compact interferometer with aperture 3 mm and 165x165 pixels [8]. The effective pixel distance (distance between neighboring measurement positions on the topography) of the interferometer is 19 µm; systematic sensor errors are in the region of 30 nm (Peak to Valley) and the sensor noise shows a standard deviation of 5 nm. Each pixel averages the topography over a width comparable to the pixel distance leading to a corresponding low pass filtering of the topography. However, for wavelengths significantly larger than the pixel averaging width these sensors can be viewed as punctual distance sensors. Lateral position of the compact interferometer has been measured with a distance interferometer and the tilt with an electronic autocollimator.

In order to study aliasing effects we proceeded as follows. The measurements made by the sensor array establish a lateral high resolution reference reconstruction [14] of the topography for wavelengths down to approximately twice of the size of the pixel distance. We then selected from the distance sensor array measurements only every 17^{th} pixel, thereby enlarging the pixel distance by factor of 17 which models the measurements by another distance sensor array having the larger pixel distance d_{pix} = 323 µm and N=8 pixels. Since the reconstruction distance is chosen equal to the pixel distance ($d_s = d_{pix}$), reconstruction of wavelengths down to 646 µm is possible. Hence aliasing can be expected in a significant part of the designed chirp specimen (cf. Fig. 5). By comparing the results obtained for this reduced sensor array with those obtained for the original measurements we can assess the amount of aliasing induced by the former for wavelengths which can be reconstructed by the original measurements but not by those of the reduced sensor array.

Figure 6 shows the two reconstruction results of the chirp specimen, one with high lateral resolution (d_s = 21 µm) serving as reference for the second using dense sampling (d_s = 323 µm).

#109895 - $15.00 USD Received 8 Apr 2009; revised 7 Jun 2009; accepted 11 Jun 2009; published 18 Jun 2009

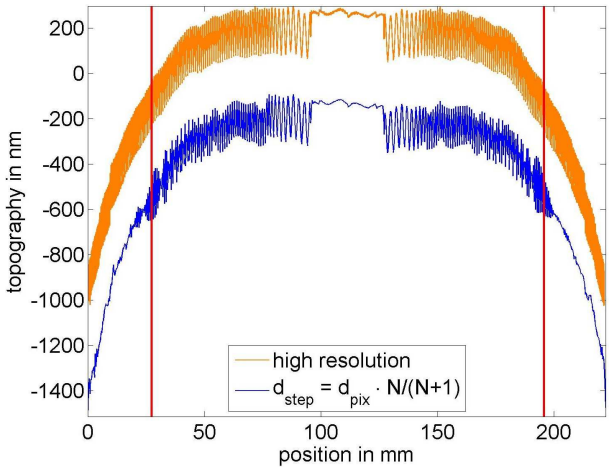

Fig. 6. Lateral high-resolution reconstruction of the entire chirp specimen utilizing all pixels of the compact interferometer (orange) and aliasing free reconstruction (blue) for dense sampling with the reduces sensor array. The red vertical lines mark the positions where the chirp specimen has a local frequency corresponding to the Nyquist frequency of the reduced sensor array.

The non-sinusoidal deviation of 1.2 µm (Peak to Valley) compared to the design function is due to the manufacturing process. This deviation is subtracted for clarity of presentation. To this end, a polynomial of degree 4 has been fitted to the high-resolution scan. This polynomial has been subtracted not only from the high-resolution scan, but also from all other profiles. Since Eq. (1) allows a reconstruction only up to an arbitrary line, all other scans have additionally been aligned to the high-resolution scan by adding a polynomial of degree one. The red vertical lines in Fig. 6 and in the following figures mark the positions in-between which the specimen consists only of wavelengths larger than $2d_s = 646$ µm, hence aliasing effects are expected to occur beyond these lines for sparse sampling.

Figure 7 and Fig. 8 show the right part of the reconstructed specimen (after subtracting its gross form). The midline of the orange high-resolution profile where the zero crossings of the sinusoidal waves are placed represents the long wavelength profile of the chirp specimen. Therefore, a profile measurement without aliasing should follow this midline when the wavelengths of the specimen become shorter than $2d_s$ (marked by the red vertical line). For the sparse sampling ($d_s = d_{pix}$, Fig. 7) the reconstructed profile is jumping up and down on the right hand side of the red line showing significant aliasing.

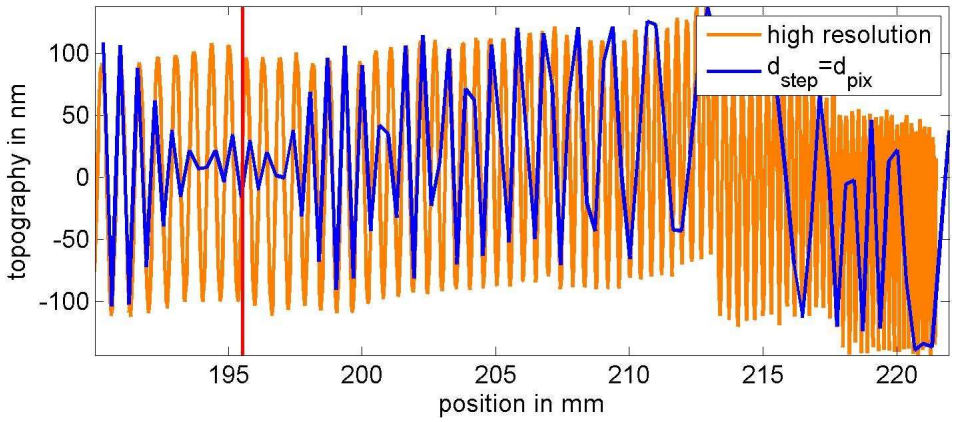

Fig. 7. Detailed view on the reconstructed chirp specimen for sparse topography sampling.

#109895 - $15.00 USD Received 8 Apr 2009; revised 7 Jun 2009; accepted 11 Jun 2009; published 18 Jun 2009

The results in Fig. 8 demonstrate that this aliasing can be significantly reduced for dense sampling.

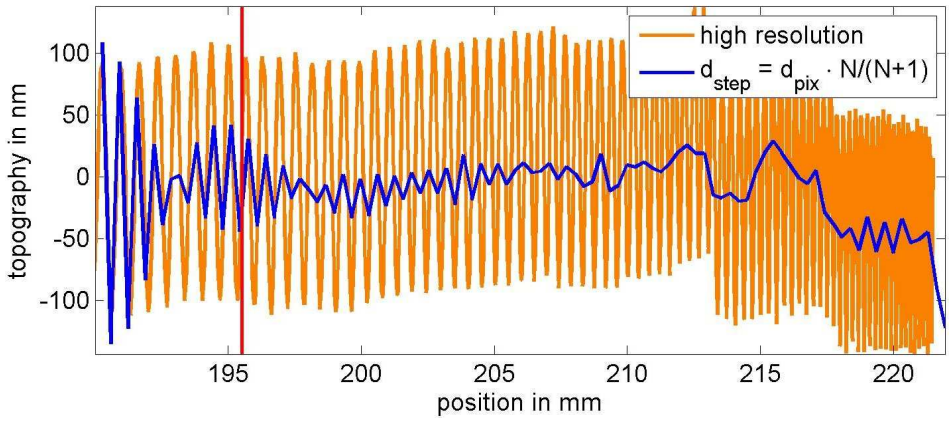

Fig. 8. Detailed view on the reconstructed chirp specimen for dense topography sampling.

The reconstructed profile is close to the midline of the chirp specimen; hence, the measured profile represents only the lower frequency part of the specimen. Recall that the blue curve in Fig. 8 is obtained by using only every 17th pixel of the data used for constructing the orange reference curve. Hence profile reconstruction with a high lateral resolution and subsequent low pass filtering is not possible to obtain the same results as in Fig. 8.

The simulations have shown that sinusoidal topographies with $f_{topo} / f_{Nyq} = 2M$ (M=1,2,3,…) lead to rms reconstruction errors larger than the amplitude of the specimen also for dense sampling. At the position x = 214.4 mm the chirp has a local frequency of $f_{topo} / f_{Nyq} = 2$ and at x = 221.05 mm local frequency of $f_{topo} / f_{Nyq} = 4$. But perhaps since the frequency of the chirp is continuously varying, aliasing effects for these singular frequencies appear to have only a minor effect.

6. Conclusion

The problem of aliasing in absolute scanning profile measurement using multi sensor scanning techniques has been considered. It was shown in terms of both, simulations and measurements, that aliasing can be reduced when the measurement locations are distributed as uniformly as possible over the specimen and when the data is analyzed in an appropriate way. Such dense sampling can be realized by a suitable choice of the scanning steps of the multi sensor array. Compared to sparse sampling, the number of scanning steps needs to be increased only by a factor of (N+1)/N where N denotes the number of distance sensors in the sensor array. Not all frequencies beyond the Nyquist frequency can be suppressed, especially even multiples of the Nyquist frequency interfere with the reconstruction algorithm and lead to large reconstruction errors. However, measurement results for a chirp specimen show that these errors for single frequencies may not be critical for a broadband topography. It is concluded that the proposed proceeding helps to improve the fabrication and characterization of high precision optical surfaces in cases where aliasing in topography form measurement can cause topography form errors by a subsequently applied post processing of the specimen.

Acknowledgments

The authors whish to acknowledge Manuel Stavridis for providing the simulation environment. Support of the Braunschweig International Graduate School of Metrology (IGSM) is gratefully acknowledged.

#109895 - $15.00 USD Received 8 Apr 2009; revised 7 Jun 2009; accepted 11 Jun 2009; published 18 Jun 2009